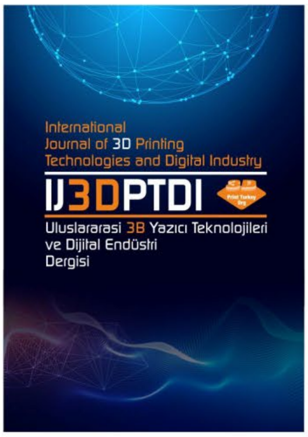

ULUSLARARASI 3B YAZICI TEKNOLOJİLERİ
VE DİJİTAL ENDÜSTRİ DERGİSİ

INTERNATIONAL JOURNAL OF 3D PRINTING TECHNOLOGIES AND DIGITAL INDUSTRY

ISSN:2602-3350 (Online)

URL: https://dergipark.org.tr/ij3dptdi

INFRARED THERMOGRAPHY IMAGE BASED CLASSIFICATION OF SOIL DIRT AND FABRIC

Yazarlar (Authors): Mehmet Deniz, Mine Seçkin, Çetin Gençer, Durmuş Koç*

Bu makaleye şu şekilde atıfta bulunabilirsiniz (To cite to this article): *Deniz M., Seçkin M., Gençer Ç., Durmuş K., "Infrared Thermography Image Based Classification of Soil Dirt and Fabric" Int. J. of 3D Printing Tech. Dig. Ind., 7(3): 441-455, (2023).*

DOI: 10.46519/ij3dptdi.1339049

Araştırma Makale/ Research Article

Erişim Linki: (To link to this article): https://dergipark.org.tr/en/pub/ij3dptdi/archive

INFRARED THERMOGRAPHY IMAGE BASED CLASSIFICATION OF SOIL DIRT AND FABRIC

Mehmet Deniz [a], Mine Seçkin [b], Çetin Gençer [c], Durmuş Koç [d]*

[a] Uşak University, Faculty of Arts and Sciences, Geography Department, TÜRKİYE
[b] Uşak University, Textile Engineering Department, TÜRKİYE
[c] Fırat University, Faculty of Technology, Electrical – Electronics Engineering Department, TÜRKİYE
[d] Isparta University of Applied Sciences University, Uluborlu Selahattin Karasoy Vocational School, Department of Computer Technologies, TÜRKİYE

* *Corresponding Author: akindurmuskoc@gmail.com*

(**Received:** 07.08.23; **Revised:** 27.09.23; **Accepted:** 12.10.23)

ABSTRACT

Soil is the substance most likely to meet nature and dirt people, vehicles, and clothing, especially in outdoor. Both source material and soil samples can be damaged during industrial and criminal investigations. Therefore, there is a need for detection, examination, and identification systems that can minimize contact with forensic evidence and provide accurate results with fewer samples. The study aims to determine the type of soil using a low-cost, easily accessible, and highly sensitive system that can be used easily without interference from the surface properties of the textile or destruction of the structure of the dirt. The working sites and areas of samples to be collected were determined according to the purpose of the study. In this context, samples of the most common soil types were taken from the lands in the Aegean Region of Turkey. Different types of substances were applied and dirtying on the collected samples. The newly formed samples were heated with a heating surface and allowed to cool. During this process, a thermal video was recorded, and feature extraction was performed. 165 samples were obtained from 55 tests. As a result, it is seen that the proposed method can detect samples with 97% accuracy.

Keywords: Thermal Image, Fabric, Non-Destructive Testing, Material, Soil, Machine Learning, Classification.

1. INTRODUCTION

In contemporary times, the significance of error, contamination, and defect analysis founded upon artificial intelligence has been progressively growing within the textile industry. Research endeavors within this domain hold substantial promise for the identification of flaws and imperfections in manufacturing processes, the enhancement of product quality, and the reduction of operational expenses. Projections articulated in this context underscore the escalating adoption of artificial intelligence, notably within the textile sector, which has historically relied upon manual labor-intensive methodologies [1-2]. Notably, the predominant arena in which artificial intelligence finds widespread application in textiles is quality control, wherein it is instrumental in the detection of production faults [3], predictive maintenance [4-5], and defect detection [6–8]. These applications are especially prevalent in quality control initiatives utilizing data modalities such as time series and image analysis.

Methods used for the analysis of textiles in the investigation of judicial cases are divided into three; mechanical, chemical, and optical investigation. Investigation of fibers after being collected from the crime scene using materials like tweezers or sticky tape sets an example to the mechanical investigation method [9]. Mechanical investigation of features such as fiber transfer, pressing of textile bodies on other materials and damage to the materials, could give important data about textile dirt. While the material on the surface of a textile can be investigated, chemical investigation is used in the detection of any chemical or fluid dirt. The major disadvantage of chemical investigation is that the sample goes into a chemical reaction and the evidence generally gets irreversibly disrupted. Using the limited number of samples and making the most efficient use of the sample investigation are the basic objectives in judicial cases. In research of Hoffman et. al. [10] studied the impacts of washing parameters used by the criminals for the spoliation of evidence and the problem of the detection method to be used in case of such washing. They managed to detect blood dirt on fabric using dyestuff and ultraviolet lighting techniques after the washing process including the effect of machine, detergent, or temperature. On the other hand, the ultraviolet lights used in this method can lead to damage to the sample if applied for an extended time and the dyestuff used to obtain a shining effect in ultraviolet light disrupts the chemical structure.

The optical investigation has become a popular area with the recent development of image processing techniques. Optical investigation methods are divided into three as basic image processing, image scaling, and image wavelength investigation. Basic image processing is the most common optical investigation method. In this method, properties of evidence like a dirt, color change, trace, and size are investigated [11–14]. These methods are fast, practical, and cost-efficient. In research, Arthur et. al. [15] tried to detect the structural characterization of blood splash and the direction of the blood on the surface in judicial cases. This method was reported to have the potential to generate quantitative data rapidly and efficiently by applying various types of blood dirt. Murray et. al. [11] conducted a research to investigate a murder case in Australia to find out how the soil was transferred to the clothing, based on the fact that the victim was attacked in the garden as there was soil on victim's clothing and there was the soil in the front garden. As the fabric dirtying method, they transferred soil to the brassiere by mainly rubbing the brassiere. The brassiere wrapped with a 2-kg weight was rubbed on the soil to obtain intact dirt patterns on the fabric without removing out the weight. Although the dragging method was the only method used in the research, a white pattern-free fabric was used to better define the image of the dirt transferred with rubbing method. In 2016, Murray et. al. [12-13] carried out a research where they tested cotton, nylon, polyester and cotton blend and the stitches and buttons of the clothing together with polyester fabric. Using the image processing method, they defined the patterns appearing on every kind of fabric and button following the transfer. In 2017, Murray et. al. [14] repeated their previous laboratory-based soil transference experiment by dragging a mannequin of 55-kg weight in areas with natural and anthropogenic soil types under both wet and dry soil conditions. 8 patterns were determined in laboratory environment whereas the transfer model set was expanded in this method by determining 12 patterns. Three studies carried out by Murray et. al showed that a plain white fabric was used to better define the pattern after the transfer. In the research carried out by the researchers in 2016, it was seen that wearing the brassiere externally and direct dragging process decrease the ecological validity of the research, and this was rarely possible to be experienced. Underwear such as brassiere are generally white or unicolored. Color separation in these kinds of fabrics can be performed with traditional image processing or color comparison methods. On the other hand, there may be various color scales and patterns in fabrics used for outerwear. For this reason, color imaging in the invisible ranges of the light spectrum rather than the traditional image processing methods is preferred.

Invisibly tiny traces, fibers, cuts, holes, etc. are investigated with scaling [16-17]. Fitzpatrick and Raven, in their investigation of the cold file of a 1983 murder, used morphological observations with the naked eye and scanning electron microscopy (SEM), chemistry, traditional laboratory A comparative study was conducted including beam diffraction (XRD) and synchrotron μ-XRD methods [17]. Robertson et. al. [16] gave examples to the mechanical investigation of forensic textile surfaces in terms of their disruption by cutting, holing, animal-based injury, rubbing, etc. When carrying out investigation by changing wavelength reactions given to infrared and ultraviolet regions are examined as well as the sensitive reactions to visible spectrum [10]. Spectroscopic analysis among the wavelength analysis methods is a process where the properties of a substance are analyzed through absorbed particles, light, or sound. This is a method determining the molecules', ions', and cores' levels of quantization of energy. It is not dependent on chemical investigation and causes no damage to the sample during investigation [9]. In their research, Kern et. al.[18] used the spectroscopy method to analyze the dirt on the trousers of an individual considered to be exposed to violence. They reported that a fast analysis could be performed using a limited number of samples with this method. Pirrie et. al [19] used the microscopic analysis in their research to detect location in forensic soil investigation. Microscopic analysis with spectroscopy provides rapid results. It can be performed with small samples and without any harm to the samples. However, the greatest disadvantage of the method is that the spectroscopy device is expensive and not easily accessible. Point analysis is performed using the spectroscopy device and only a single point on the sample is examined. Chang et. al. addressed the advantages and disadvantages of Fourier-transform infrared spectroscopy (FTIR), Raman spectroscopy and elemental analysis methods used in forensic investigations [20-21]. The thermal imaging system is one of the alternative methods used in forensic investigation. Evidence regarding the temperature traces-patterns remaining on the materials in the crime scene or whether they were used can be revealed with this method [22]. Mapping temperature change/cooling of body parts [23] and vascular pattern recognition [24] set examples to forensic medicine practices. Heating with a light source, chopping mechanism, and thermal camera systems are developed to investigate samples to view the contrasts of chemicals [25-26]. Unlike spectroscopic analysis, the sample is not damaged in image processing, and it can be reused more than once. However, soil color with image processing in colored fabrics could generate inaccurate results. The aim of the study is to develop a cost efficient, color-independent, and easily applicable system for the analysis of the fabrics as the spectroscopy device is costly, the image processing technique has certain disadvantages like causing troubles in the analysis of colored fabrics and no example of the use of thermal camera in analysis in the literature.

Non-destructive testing (NDT) includes all techniques such as imaging, classification, or segmentation using techniques such as acoustic, optoelectronic, capacitive, and electromagnetic methods that are used to detect defects, contaminants, and foreign materials without affecting the function or reliability of the material. NDT methods include important optical methods used to detect defects and dirt in fabrics. These methods focus on detecting fabric surface imperfections, defects, or dirt without destroying them. Among the optical methods, techniques such as visual inspection, image processing [8, 27], infrared (IR) [28-29] imaging and ultraviolet (UV) [6] illumination offer effective tools to detect defects without disrupting the structural integrity of fabrics and disrupting production processes. In this way, quality control and product evaluation processes in industrial and commercial areas become more efficient and reliable. NDT is commonly used in the composite material or metal fabrication industry to understand and evaluate the properties, condition and quality of tested objects for quality control purposes [30–33]. Conventional NDT testing methods mainly consist of methods for measuring the reflection, absorption, or penetration of signals emitted from a signal source from the sample under test and inspecting them with an image.

In post-event crime scene investigations, any material that would help clarification of the event either directly or indirectly is considered as evidence. Many disciplines such as chemistry, mechanics, textiles, electronics, computers, history, geography, and psychology are used in crime scene investigation, evidence collection and analysis processes [34–37]. Investigation of judicial processes consists of four basic steps as the collection of evidence, visual inspection, chemical analysis, and mechanical analysis, respectively. Everything in a crime scene that could possibly have an evidential value must be collected in the fastest and most intact manner. During the visual inspection, the evidence is examined in terms of various aspects such as structure, color, dirt, and damage. When it is not possible to obtain sufficient information through visual inspection, interaction with chemicals is studied and/or mechanical investigation is performed to gain in-depth information to understand the reason behind the change. Although the evidence must not get lost or disrupted during these processes, the structure of the evidence generally gets disrupted following chemical and mechanical analysis. Therefore, chemical and mechanical analyses are performed in the final part of the evidence inspection process [21, 34].

The study aims to develop a new, practical, and cost-efficient method for the detection of soil-based dirt on textile surfaces as well as the detection of the soil type. Expected goals and contributions of the system are listed as follows:

- ✓ It can identify soil type with high accuracy without disrupting the structure of soil-based dirt.
- ✓ It is a visual system that is not affected by parameters like a pattern or paint on the textile surface.
- ✓ It is an easily accessible system with reasonable cost compared to systems like spectroscopes.
- ✓ The system is affordable and accessible and can easily be operated by the police and forensic scientists.

In the following sections of the study, the related studies, materials, and methods used are presented in this study, respectively. Afterward, the results are discussed, and the conclusion part is presented.

2. MATERIAL AND METHOD

The general method to be followed within the scope of the study is shown in Figure-1. Accordingly, first, fabric and soil samples are collected. Then, fabric samples are dirtied with soil samples. Thermal video is recorded when heating and cooling the dirtied samples on the surface. Time-histogram features of the temperature change on the dirtied area are extracted from the thermal video recording. The features obtained are subjected to machine learning and the great soil types are classified. In the following parts of the study, sample collection, heating, and thermal recording system, video processing and machine learning-based classification processes are presented in detail, respectively.

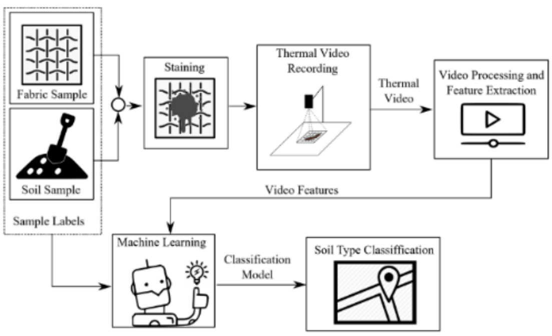

Figure 1. General method flowchart.

2.1. Soil Samples

Uşak province in Turkey was selected as the research field thanks to the rich diversity of its soil. Lands on the site change from an approximate height of 430 m up to 2309 m in Kartaltepe (Mount Murat). Besides, the site has a transition climate, leading to diversification of the plant cover and climatic conditions affecting the soil generation. When topography, geology, hydrography, and elevation factors were considered, favorable conditions were formed for the observance of 11 different great soil groups in this area. The main soil types observed in this area according to the 1949 American soil classification system were included in the research which is presented in Table 1 according to 1949 Soil Classification [38] and samples are shown in Figure 2. The soil maps prepared by the Turkish Republic Prime Ministry General Directorate of Rural Services for Agricultural Usage according to 1949 Soil Classification has been used during the mapping process. The locations and distribution of soil types in Uşak province are shown in Figure 3. This classification was developed in 1949 by Guy D. Smith and James Thorp [38], but is still used today in Turkey. This classification was preferred as it is the most valid type of classification used in soil mapping in Turkey. ArcGis 10.2 software was used for drawing maps. Samples used in the research were collected from horizons O and A forming top soil, which were more likely to leave dirt in case of contact with clothes. Other horizons were not included in the sample group as they had a fewer probability of contact. Particular attention has paid to the fact that soil samples to be collected were from the locations to be best representing the relevant great soil group. Sites with a height varying from 500m to 1100m, representing the land in general, were considered while selecting the samples.

Figure 2. Soil samples.

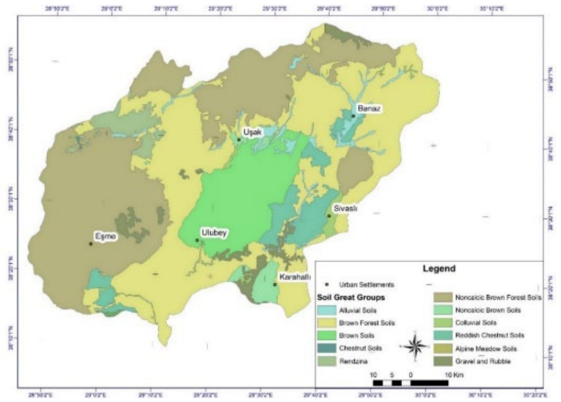

Figure 3. Soil sample map.

The soil at all levels of lime accumulation from low to high are available throughout the province [39]. All samples collected from the site involved lime. Therefore, all soils reacted with acid while the level was rather low in alluvial soils (Table 2). 86% of the soil used in agriculture in the research site contains a high amount of potassium. pH reaction of soil is of alkali nature in 79% and is neutral in 18%. Most of the soil is clay loamy, corresponding to 51%. 43% of the soil is loamy [39]. In terms of soil texture, soils vary from easily crumbling sandy soil to clay loam, even clay deposits are encountered (Table 2). In terms of granular size and collection, soil types varying from platy to single granular soil are observed. 77% of the soil in the province is poor or very poor in organic substances whereas 76% of them are poor or very poor in phosphor (P2O5) [39]. The color of soil was mainly affected by the minerals they contain, the climate and its structure. The Munsell color system was used in the color determination. The color determination was performed by the researchers. It was observed that there was soil in several different colors from dark red to green. Organic substances were abundant in all samples and horizons O and A had a darker color (Table 2). A different land cover was formed on the samples collected from the research site (Table 3). Steppe plants and forests are widespread particularly on steep or arid lands where agriculture is difficult. Samples of agricultural sites, as well as naturally grown forests, are available. The natural plant cover is preserved in all non-agricultural areas of the sample sites. Oak and red pine trees (Pinus brutia Ten.) are widespread in the woodlands where the samples are collected. As for the land's forests are unable to grow, continental climate is observed in higher areas while plant communities of the Mediterranean climate are found in lower areas.

Table 1. Properties of soil samples.

Sample No	Great Soil Groups	Soil Order	Soil Suborder	Classification (1974)	Pedogenic Process
S01	Noncalcic Brown Forest Soils	Zonal	Soil of the forest-grassland transition	Cambisols	Decalcification
S02	Brown Forest Soils	Intrazonal	Calsimorfic	Cambisols	Calcification & sedimentation
S03	Rendzina	Intrazonal	Calsimorfic	Rendzina, Leptosol	Calcification
S04	Chestnut	Zonal	Dark-colored soils of semiarid sub humid and humid grassland	Kastanozems	Calcification
S05	Rendzina (Clay rich)	Intrazonal	Calsimorfic	Rendzina	Calcification
S06	Andosol	Azonal	-	Andosol	Weathering, mineral transformation, hydrolysis & decalcification
S07	Brown soils	Zonal	Light colored soils of arid regions	Cambisols	Calcification
S08	Colluvial Regosols	Azonal	-	Arenosols	Alluvium and colluvium
S09	Reddish Chestnut	Zonal	Dark-colored soils of semiarid sub humid and humid grassland	Kastanozems	Calcification & oxidation of Fe
S10	Alluvial	Azonal	-	Fluvisols	Alluvium & colluvium
S11	Noncalcic Brown soils	Zonal	Soil of the forest-grassland transition	Luvisol	Decalcification

Table 2. Physical components of soil samples.

Sample No	Altitude (m)	Munsell Color	Acid Reaction	Texture	Structure
S01	909	10R (3/6) Dark Red	+	Silty Clay Laom	Single granular
S02	783	7,5YR (4/6) Strong Brown	+	Sandy Laom	Single granular
S03	743	7,5 YR (6/3) Light Brown	+	Silty Clay Laom	Platy
S04	762	10R (3/3) Dusky Red	+	Silty Clay Laom	Single granular
S05	616	5Y (5/2) Olive Gray	+	Silty Clay	Single granular
S06	574	10R (5/2) Weak Red	+	Clay Laom	Single granular
S07	978	7,5 YR (4/4) Brown	+	Clay Laom	Single granular
S08	1059	7,5 YR (5/4) Brown	+	Sandy Laom	Granular
S09	929	10R (4/4) Weak Red	+	Silty Clay Laom	Single granular
S10	879	7,5 YR (2,5/3) Very Dark Brown	+	Clay loam	Single granular
S11	918	2,5 YR (2,5/4) Dark Reddish Brown	+	Silty Clay Laom	Single granular

Table 3. Land use properties on soil samples areas.

Sample No	Land Use	CORINE Land Cover Class	CORINE Land Cover Nomenclature
S01	Agriculture	Non-irrigated arable land	211
S02	Forest (Pinus brutia)	Coniferous forest	312
S03	Forest (Quercus cerris L.)	Broad-leaved forest	311
S04	Agriculture	Non-irrigated arable land	211
S05	Forest (Quercus cerris L.)	Broad-leaved forest	311
S06	Forest (Quercus cerris L.)	Broad-leaved forest	311
S07	Agriculture	Non-irrigated arable land	211
S08	Forest (Junperus oxycedrus L.)	Mixed forest	313
S09	Agriculture	Non-irrigated arable land	211
S10	Agriculture	Permanently irrigated land	212
S11	Agriculture	Non-irrigated arable land	211

2.2. Fabric Samples

Textile surfaces are divided into three groups as knitted, woven and nonwoven surfaces. Knitted shirt fabrics were used in this research. Woven fabrics contain 3 different types of weaving as plain weave, twill, and satin. Woven shirt fabrics used in this research are made of the blend of these types of weaving and are shown in Figure 4. Fabrics have different parameters of composition, design, color, and weight, which are shown in Table 4 in detail. Design/color indicates the design and colors of the samples. Weight means the fabric's gram weight per square meter. Composition means the blending proportion of different types of fibers making up the fabric. Sample 1 is a 160 gr/m2 blend of cotton polyester and elastin in black and white design. Sample 2 is a 115 gr/m² blend of lycra and cotton in a red and white plaid design. Sample 3 is a 210 gr/m² blend of polyester and elastin in indigo plaid design. Sample 4 is a 200 gr/m² brown satin and cotton fabric. Sample 5 is a 165 gr/m² dark blue cotton plaid fabric.

Figure 2. Image of fabric samples.

Table 4. Properties of fabric samples

Sample No	Design/Color	Weight (gr/m²)	Composition (%)
T01	Black and White	160	49% Cotton + 49%Polyester+ 2%Elastin
T02	Red and White plaid	115	30%Lycra+ 70% Cotton
T03	Indigo plaid	210	48%Cotton + 47%Poliester + 5%Elastin
T04	Brown satin	200	100%Cotton
T05	Blue plaid	165	100%Cotton

2.3. Dirtying Process

Like the method used by Murray et. al.[11–13] rubbing against soils with a certain amount of weight was applied in this research (Fig. 5). The method can also be used by the police and forensic scientists as a cost-efficient and easily applicable forensic soil investigation method. Fabric samples are dirtied with soil samples using the system presented in Figure 5. First, soil samples collected from 11 different regions were conditioned at room temperature in this research. 55 dirtying processes were performed on 5 different fabric samples using soil samples collected from 11 different regions of Uşak province. As seen in Figure 5-a and Figure 5-b, the fabric was tightly wrapped using a handle with the help of a pin. Fabric that was tightly fixed on the handle was placed into the area arranged in the handle section with a 2 kg weight on it as seen in Figure 5-c and Figure 5-d. Inside the dirtying pool, the fabric with weight was rubbed from left to right for 2 minutes with the help of the handle as seen in Figure 5-e. Upon the completion of the dirtying process, the fabric was separated from the handle as seen in Figure 5-f. When the dirtying process was ended, the fabric sample was placed on the heater surface.

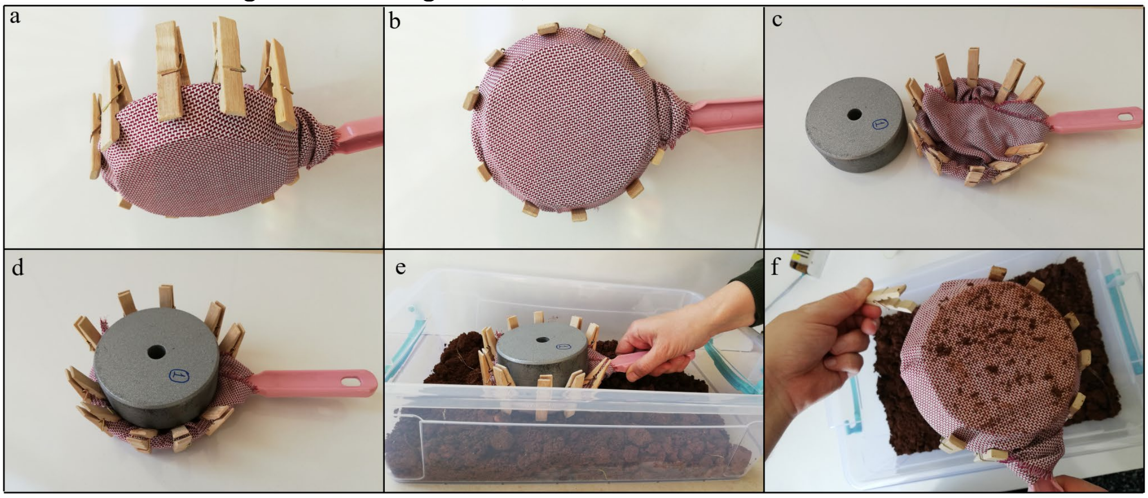

(a) (b) (c) (d) (e) (f)

Figure 3. Fabric dirtying method steps: a- Wrapping the fabric around the handle tightly with the help of a pin, b- Image of the fabric before the dirtying, c- Preparing 2 kg weight, d- Placing a 2 kg weight on the fabric, e- Rubbing the fabric with a weight against soil from the left to the right for 2 minutes, f- Separating the fabric dirtied with soil.

2.4. Thermal Non-Destructive Test Setup

As is seen in Figure-6, the thermal NDT system consists of a thermal investigation unit, thermal camera, power source, heater controller and a heater surface. After the dirtying process, the fabric sample de-attached from the 2kg weight and the handle. The dirtied fabric sample is placed on the heating surface. The heater surface is a 30x30 cm resistive plate, which can be adjusted up to 150 °C with a direct current (DC) applied from the power source. The power supply can supply a 12V 12A DC from alternating current and provides power to the heater unit with the help of the heater controller in the system. There is a thermistor temperature sensor in the middle of the heater surface. The value measures on the temperature sensor are sent to the heater control unit for feedback. The heater control unit ensures that the heater surface remains in the desired temperature with the Proportional Integral Derivative (PID) control [40]. Arduino Mega and Ramps 1.4 circuit is used as a control unit [41]. The heater control unit is connected to the thermal investigation unit with a USB and the desired temperature is adjusted on the Thermal Investigation Unit. The thermal camera is of Testo 871 brand and model. The thermal camera can deliver live stream. The thermal camera is directly connected to the thermal investigation unit through Wi-Fi. As is shown in Figure-7, the thermal experiment process occurs first in heating, then in the cooling process. Yet, samples are kept at 25°C room temperature with 45±10% humidity rate for at least 30 min. before the thermal experiment. In the heating process, the sample is placed on the heater surface. The heater is heated up to 40°C from 25°C. It takes around 13 seconds for the heater surface to increase up to 40°C from 25°C without a sample on it. The heating process takes 1 min. In this process, the time reaching up to 40°C varies. The temperature of the heater is adjusted to 25°C following the waiting process and the sample is kept for cooling for 1 minute. It takes around 24 seconds for the heater plate to cool down to 25°C from 40°C without a sample on it.

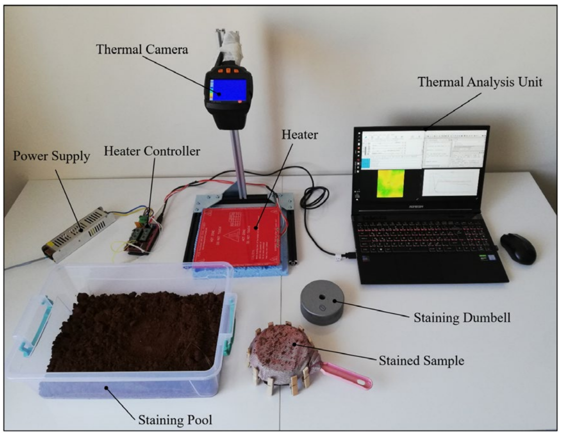

Figure 4. Thermal investigation setup.

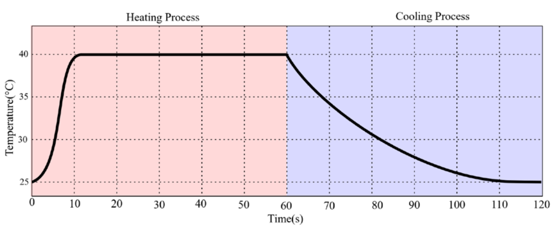

Figure 5. Heating and cooling process.

2.5. Thermal Image Processing and Feature Extraction

Images received from the thermal camera were recorded with 30 squares per second. Temperature values in thermal video images are shown with the grey color map. In the gray color map, lower temperature values are represented by black, intermediate values are represented by gray and higher temperature values are represented by white color. The temperature scale is fixed during thermal image recording, the lowest temperature adjusted as 25 whereas the highest temperature value is adjusted as 40 degrees. A sample recording obtained during the recording of a dirtied fabric is displayed in Figure-8.

Feature extraction from histogram expected values of the image was performed to monitor the time-bound change of the video record taken throughout the thermal investigation process and to extract features. Equation 1 was used for the expected value calculation. Pixel values are the single channel on the grayscale, changing from 0 to 255. The value obtained with the multiplication of each pixel value's probability value P(x) in the image, gives E[x], which indicates the expected value of the image. The expected value change in heating and cooling processes in a sample image is shown in Figure-9. Two types of feature extraction were performed: the statistical feature extraction from the signal coming out of the time-bound change of the expected values and utilization of the parameters of curve fitting as a feature.

$$E[x] = \left(\sum_{x=0}^{255} x * P(x)\right), \qquad (1)$$

Statistical features are maximum, minimum, mean, standard deviation, Root Mean Square (RMS), Crest, Kurtosis and Entropy values. These values are calculated individually for heating and cooling processes, making up a total of 14 features which are presented in Table-5. These calculations are made over time series of N number of x values. As is seen in Figure-9, there are slight fluctuations in heating and cooling processes. Curve fitting was used for this purpose to extract the characteristic state of data. Two curve fitting functions are used for feature extraction: logistic function in the heating section of the graph and exponential function in the cooling section. The logistic function h(t) used in the heating section is presented in Equation-2. Here, t is used as the time variable, e as the natural logarithm, ah as the maximum value of the curve, b_h as the logistic growth rate and c_h as the mid-point of sigmoid. In the cooling section, the negative mark in front of the b value in the same equation is changed to positive. In the cooling section, c(t) presented in curve fitting function

Equation-3 is used. Here, t is used as the time variable, e as the natural logarithm, a_c as the exponential multiplier, b_c as the exponential growth rate and cc as the offset value.

$$c(t) = a_c \times e^{-b_c \times t} + c_c, \quad (2)$$

$$h(t) = \frac{a_h}{1+e^{-b_h \times (t-c_h)}} \quad (3)$$

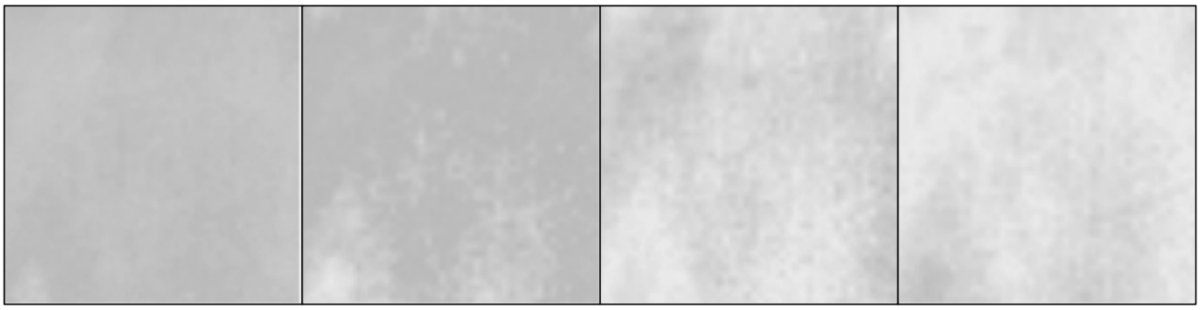

t=0s t=15s t=30s t=45s

Figure 6. Dirtied fabric thermal image

Table 5. The statistical features.

Feature	Equation	Explanation
Maximum	max(x)	Maximum value of histogram expected value time series
Minimum	min(x)	The minimum value of histogram expected value time series
Mean	$\mu = \frac{1}{N}\sum_{i=1}^{N} x_i$	Sum of all x values divided by the number of values N
Standard Deviation	$\sigma = \sqrt{\frac{1}{N-1}\sum_{i=1}^{N}(x_i - \mu)^2}$	The Standard Deviation is a measure of the amount of dispersion of x values
Root Mean Square	$x_{RMS} = \sqrt{\frac{1}{N}\sum_{i=1}^{N} x_i^2}$	The square root of the mean square of x values
Crest Factor	$C = \frac{\lvert x_{peak} \rvert}{x_{RMS}}$	Crest factor indicates how extreme the peaks are in an N length x time series
Kurtosis	$K = \frac{\sum_{i=1}^{N}(x_i - \bar{x})^4}{(N-1)s^4}$	Kurtosis describes the shape of a probability distribution of x values.
Entropy	$H = -\sum_{i=1}^{N} P(x_i) \times \log_2 P(x_i)$	The entropy can also be interpreted as the average rate at which information is produced by data.

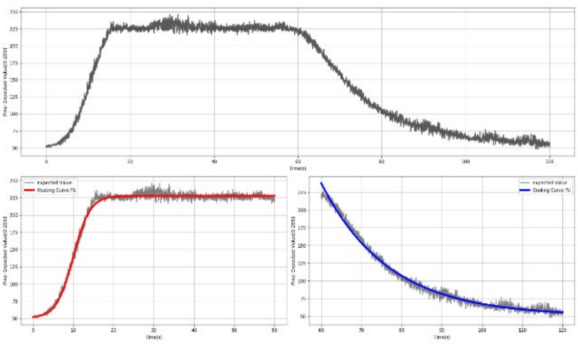

Figure 7. Curve fitting based feature extraction.

2.6. Classification With Machine Learning

The machine learning methods used in the study are summarized in Figure 10. The performance characteristics of statistical and curve fitting features which are used as input parameters were first used separately and their performance was examined, and then better characteristics were selected as a hybrid feature set from these two feature sets. The methods K-Nearest Neighbors (KNN) [42], Decision Tree (DT) [43], Random Forest (RF) [44, 45] and Adaptive Boosting (AdaBoost) [46, 47] were used as learning algorithms. K-fold cross-validation is a method used in the performance evaluation of learning algorithms [48, 49]. In this study, the K value was chosen as 10. The performance metrics of classification are chosen as accuracy, precision, F1 and Recall which are outlined in Table 6 [3, 50, 51]. TN, TP, FN and FP values are the numbers of true negatives, true positives, false negatives and false positives in confusion matrix [52].

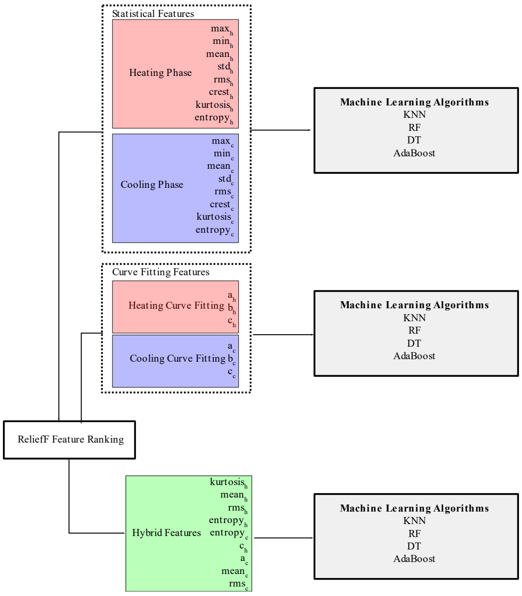

Figure 8. Machine learning inputs.

Table 6. Classification metrics.

Metric	Equation
Accuracy	$A = \frac{TN + TP}{TP + TN + FP + FN}$
Precision	$P = \frac{TP}{TP + FP}$
F1 Score	$F1 = \frac{P + R}{2}$
Recall	$R = \frac{TP}{TP + FN}$

2.7. Relief-F Feature Ranking

Relief algorithms are based on evaluating features by measuring distances between adjacent samples [53, 54]. In the Relief-F ranking algorithm, a W vector whose attribute number is n length is created to store the weight values of the features. This value is calculated for each attribute. The ReliefF score of the feature is obtained from samples. Firstly, random sample selection is made within the iterations. If the sample closest to the selected sample is in the same class, it is labelled as "hit" otherwise it is labelled as "miss". In the next step of the algorithm, the nearest "hit neighbor" and the nearest "miss neighbor" are found. For each feature, the W weight vector is updated by performing the operation in Equation-4. Here j gives the feature number and i gives the iteration number. diff (feature, sample1, sample2) calculates the difference between two different samples within the same feature. This value takes the value 0 or 1 in categorical data and takes the value in the range [0 1] for numerical values. By dividing by the value of m, all Wi values are kept within the range of [-1 1] [41]. In this study, Euclid's norm is used as a distance criterion in Relief algorithms, but the Manhattan norm is also used in ReliefF algorithm.

$$W_j^i = W_j^{i-1} - diff(A,R,H)/m + diff(A,R,M)/m, \quad (4)$$

3. RESULTS AND DISCUSSION

The method and system developed within the framework of the purpose, 11 soil samples, and 5 fabric samples, making up a total of 55 sample dirtying processes, were available. Each sample was calculated 3 times, leading to a total of 165 data. 8 statistical and 6 curve fittings were used to extract features from each sample. Correlation values the features obtained corresponding to the relevant soil type and the fabric type are presented in Figure-11. Considering these values, $mean_h$, std_h and $entropy_h$ respectively, are the three variables with the highest correlation coefficient for soil type.

The effect of composition and weight features of the fabrics on the rate of temperature change was examined in the study. The rate of temperature change occurring in the first 10 seconds of the heating process on fabric type basis is shown in Figure-12. The values represent the mean value of the expected value change per second within the first 10 seconds. It can clearly be seen from the graph that the heating ratio of 49% and 47% polyester samples in unit time is higher compared to others. In terms of weight, it is seen that higher weight fabrics generally get heated in a faster manner. In Figure-11, fabric sample No 3 is the type of fabric heated the fastest with a value of 23.782 E(x)/sec. The type of fabric heated the slowest is the fabric sample no 5, with a value of 22.687 E(x)/sec. Literature has presented results indicating that temperature change of fabrics should be faster with the increase in the amount of polyester and a decrease in weight. Yet, these results cannot be seen directly in Figure-12 [56]. For example, although sample 3 was heated faster than sample 1, Figure-12 showed that it got heated slower. This is because samples are dirtied with soil. Temperature changes of dirtied and raw fabrics will be measured in future studies.

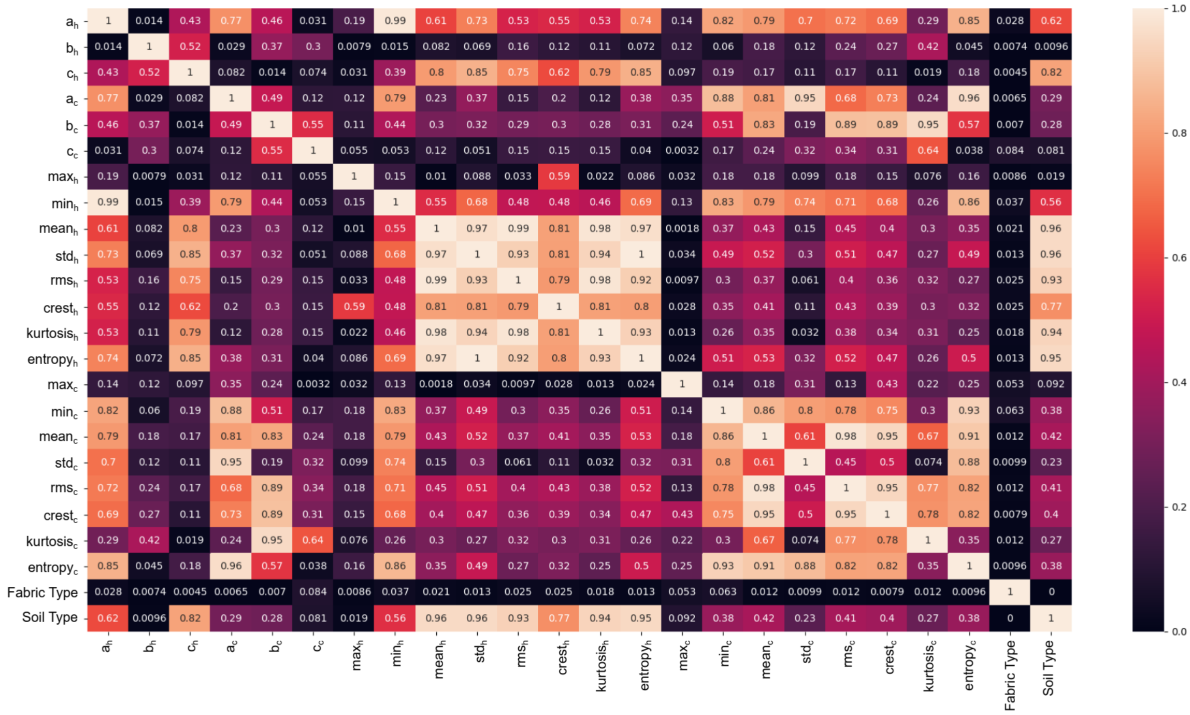

Figure 9. Feature absolute cross-correlations coefficients.

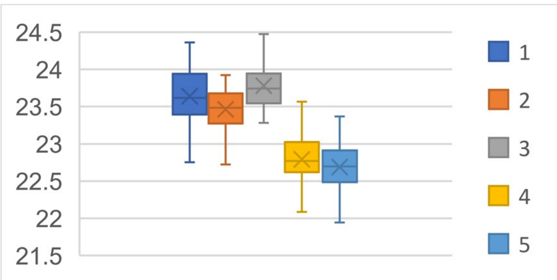

Figure 12. Heating maximum value comparison according to fabric type.

Three different feature clusters were compared for classification with ensemble machine learning. 14 statistical features were used in the first feature cluster. 6 features obtained with curve fitting were used as the second feature cluster. A hybrid feature cluster was prepared as the last feature cluster. While determining the hybrid feature set, 10 features with the highest score are selected by using ReliefF feature ranking method. ReliefF scores of all features are shown in Figure-13. The features selected according to the ReliefF score are $kurtosis_h$, $mean_h$, rms_h, std_h, $entropy_h$, $entropy_c$, c_h, a_c, $mean_c$ and rms_c, respectively. The $kurtosis_h$ feature, the largest in the selected attribute set, has a score of 0.331. Table-7 presents the training time, accuracy, f1, precision and recall metrics obtained with the application of the learning process 5-fold cross-validation by using the statistical, curve fitting and hybrid features with RF and AdaBoost Learning Algorithms. When the Table is examined, it is seen that the RF algorithm using hybrid features has the highest accuracy value of 0.976 while the KNN algorithm using curve fitting feature has the lowest accuracy value of 0.703. The confusion matrix of the RF algorithm using a hybrid feature possessing the highest accuracy value is presented in Figure-14. Accordingly, the highest number of false estimations was 4.

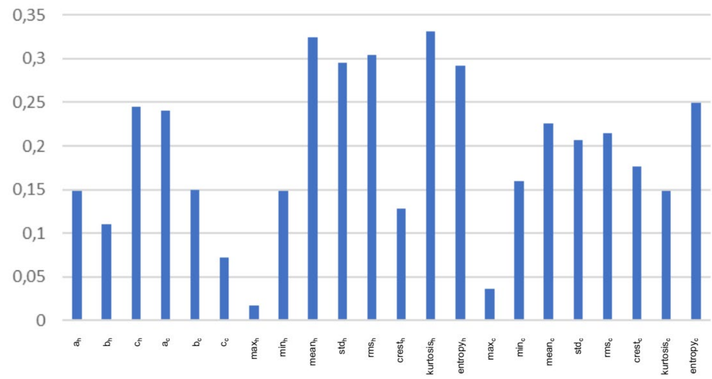

Figure 10. Feature relief-f ranking scores.

Table 7. Performance metrics according to features and learning algorithms.

Feature	Algorithms	Training Time	Performance Metrics			
			Accuracy	F1	Precision	Recall
Statistical	AdaBoost	0.031	0.903	0.903	0.904	0.903
	KNN	0.022	0.939	0.939	0.946	0.939
	RF	0.081	0.964	0.963	0.965	0.964
	DT	0.052	0.861	0.859	0.868	0.861
Curve Fitting	AdaBoost	0.024	0.855	0.855	0.858	0.855
	KNN	0.016	0.703	0.699	0.711	0.703
	RF	0.074	0.933	0.933	0.934	0.933
	DT	0.044	0.788	0.789	0.796	0.788
Hybrid	AdaBoost	0.026	0.891	0.891	0.893	0.891
	KNN	0.019	0.958	0.957	0.962	0.958
	RF	0.076	0.976	0.976	0.977	0.976
	DT	0.042	0.873	0.871	0.877	0.873

Predicted

Actual	1	2	3	4	5	6	7	8	9	10	11	Σ
1	14	0	0	0	1	0	0	0	0	0	0	15
2	0	15	0	0	0	0	0	0	0	0	0	15
3	1	0	14	0	0	0	0	0	0	0	0	15
4	0	0	0	15	0	0	0	0	0	0	0	15
5	1	0	0	0	14	0	0	0	0	0	0	15
6	0	0	0	0	0	15	0	0	0	0	0	15
7	0	0	0	0	0	0	15	0	0	0	0	15
8	0	0	0	0	0	0	0	15	0	0	0	15
9	0	0	0	0	0	0	0	0	15	0	0	15
10	0	0	0	0	0	0	0	0	0	15	0	15
11	0	0	0	0	0	0	0	1	0	0	14	15
Σ	16	15	14	15	15	15	15	16	15	15	14	165

Figure 11. Confusion matrix of RF learning algorithm using hybrid features.

4. CONCLUSIONS

The aim of the study is to develop a new, practical, and cost-efficient NDT method for the detection of soil-based dirts on textile surfaces as well as the detection of the soil type. In line with this aim, fabric samples tightly wrapped around the handle are dirtied in the dirtying pool with a 2 kg weight. The sample is then removed out of the dirtying pool and placed on the heater surface of the thermal investigation system. The value measured with a thermistor temperature sensor in the middle of the heater surface is delivered to the control unit for feedback. The thermal experiment process consists of an initial heating and a subsequent cooling process. This method is more cost-efficient than other systems like spectroscopy. In this system, soil type could be identified with a high accuracy rate without being affected by parameters like the pattern or dye and without disrupting the structure of the soil-based dirt. Moreover, the system can be easily applied by forensic scientists.

Soil and fabric effects were assessed through 165 measurement results of 55 different tests and 3 separate measurements from each test in the study. The effect of fabric composition and weight on heating time was examined and it was observed that fabric composition affected the change of value. The graph clearly shows that polyester samples get heated more in unit time compared to others. Results like those in the literature that characterize the thermal comfort properties of fabrics with different test devices were obtained within the thermal camera. This provides more economical and innovative horizons with thermal imaging systems instead of expensive thermal comfort test equipment. The type of fabric that gets heated the slowest is fabric sample No 5. Moreover, the temperature change in fabrics was fast as expected in the literature. However, this sample is not the same as the sample fabric dirtied with soil. Temperature changes of dirtied and raw fabrics will be measured in future studies.

Three different feature clusters were compared for classification with ensemble machine learning. The RF algorithm using hybrid features has the highest accuracy value of 0.976 while the KNN algorithm using hybrid features has the lowest accuracy value of 0.703. According to the most accurate RF algorithm using hybrid features, the highest number of wrong estimations was 4. This accuracy value is very high and shows that almost all the soils can be classified precisely. Estimating the existing soils in Uşak province and the number of fabric samples are among the limitations of the research. It is planned to conduct future studies by increasing the number of soil and fabric samples. Despite this, in the study, the classification of soils in Uşak province was completed with high performance values regardless of the fabric type. It will contribute to the literature if future researchers increase the number of soil and fabric samples and expand the study to different regions, unlike this study conducted with regional samples.

ACKNOWLEDGEMENT
This research received no external funding. The authors declare no conflict of interest.

REFERENCES
1. Tansan, B., Gökbulut, A., Targotay, Ç., Eren, T., "Industry 4.0 in Turkey as an Imperative for Global Competitiveness Report", https://tusiad.org/tr/yayinlar/raporlar/item/download/7848_180faab86b5ec60d04ec929643ce6e45, September 26, 2016.

2. Küsters, D., Praß, N., Gloy, Y.S., "Textile learning factory 4.0–preparing Germany's textile industry for the digital future", Procedia Manufacturing, Vol. 9, Pages 214–221, 2017.

3. Seçkin, M., Seçkin, A.Ç., Coşkun, A., "Production Fault Simulation and Forecasting from Time Series Data with Machine Learning in Glove Textile Industry", Journal of Engineered Fibers and Fabrics, Vol. 14, Pages 1-12, 2019.

4. Chang, R.I., Lee, C.Y., Hung, Y.H., "Cloud-based analytics module for predictive maintenance of the textile manufacturing process", Applied Sciences, Vol. 11, Issue 21, Pages 1-22, 2021.

5. Shamsuzzaman, M, Mashud, M., Rahman, M. M., Rahman, M.M., Hoq, E., Das, D., "Management and maintenance of textile machinery", Rahman, M. M., Mashud, M., Rahman, M.M. et al editors, Advanced technology in textiles, Pages 31-63, Springer Nature, Singapore, 2023.

6. Bandara, P., Bandara, T., Ranatunga, T., Vimarshana, V., Sooriyaarachchi, S., Silva, C.D., "Automated fabric defect detection", 2018 18th International Conference on Advances in ICT for Emerging Regions (ICTer), Papes 119–125, Sri Lanka, 2018.

7. Li, C., Li, J., Li, Y., He, L., Fu, X., Chen, J., "Fabric defect detection in textile manufacturing: a survey of the state of the art", Security and Communication Networks, Vol. 2021, Pages 1-13, 2021.

8. Seçkin, A.Ç., Seçkin, M., "Detection of Fabric Defects with Intertwined Frame Vector Feature Extraction", Alexandria Engineering Journal, Vol. 61, Issue 4, Pages 2887-2898, 2022.

9. Morison, R., "Improving the forensic value of textiles and fibres through the holistic detection and analysis of acquired characteristics due to environmental factors", PhD Thesis, University of Technology, Sydney, 2019.

10. Hofmann, M., Adamec, J., Anslinger, K., Bayer, B., Graw, M., Peschel, O., Schulz, M.M., "Detectability of bloodstains after machine washing", International Journal of Legal Medicine, Vol. 133, Issue 1, Pages 3–16, 2019.

11. Murray, K.R., Fitzpatrick, R.W., Bottrill, R.S., Berry, R., Kobus, H., "Soil transference patterns on bras: image processing and laboratory dragging

experiments", Forensic Science International, Vol. 258, Issue 2016, Pages 88–100, 2016.

12. Murray, K., Fitzpatrick, R., Bottrill, R., Kobus, H., "Soil transference patterns on clothing fabrics and plastic buttons: image processing and laboratory dragging experiments", Forensic Science and Criminology, Vol. 2, Issue 1, Pages 1–12, 2016.

13. Murray, K.R., Fitzpatrick, R.W., Bottrill, R., Kobus, H., "An investigation of the pattern formed by soil transfer when clothing fabrics are placed on soil using visual examination and image processing analysis", Forensic Science and Criminology, Vol. 2, Issue 1, Pages, 1–11, 2017.

14. Murray, K.R., Fitzpatrick, R.W., Bottrill, R., Kobus, H., "Patterns produced when soil is transferred to bras by placing and dragging actions: the application of digital photography and image processing to support visible observations", Forensic Science International, Vol. 276, Issue 2017, Pages 24–40, 2017.

15. Arthur, R.M., Humburg, P.J., Hoogenboom, J., Baiker, M., Taylor, M.C., de Bruin, K.G., "An image-processing methodology for extracting bloodstain pattern features", Forensic Science International, Vol. 277, Pages 122–132, 2017.

16. Macarthur, S., Hemmings, F. J., "Fibres, yarns and fabrics: an introduction to production, structure and properties", Robertson, J., Roux, C., Wiggins, K.G. et al editors, "Forensic examination of fibres third edition", Pages 1-59, CRC Press, London, 2017.

17. Fitzpatrick, R.W., Raven, M.D., "The forensic comparison of trace amounts of soil on a pyjama top with hypersulfidic subaqueous soil from a river as evidence in a homicide cold case", Fitzpatrick, R.W., Raven, M.D. et al editors, Forensic soil science and geology, Pages 197-218, The geological society, London, 2019.

18. Kern, S.E., Crowe, J.B., Litzau, J.J., Heitkemper, D.T., "Forensic analysis of stains on fabric using direct analysis in real-time ionization with high-resolution accurate mass-mass spectrometry", Journal of Forensic Sciences, Vol. 63, Issue 2, Pages 592–597, 2018.

19. Pirrie, D., Dawson, L., Graham, G., "Predictive geolocation: forensic soil analysis for provenance determination", Episodes Journal of International Geoscience, Vol. 40, Issue 2, Pages 141–147, 2017.

20. Chang, W.-T., Chen, T.-H., Yu, C.-C., Kau, J.-Y., "Comparison of embedding methods used in examining cross-sections of automotive paints with micro-fourier transform infrared spectroscopy", Forensic Science Journal, Vol. 1, Issue 1, Pages 55–60, 2002.

21. Lewis, P.R., Reynolds, K., Gagg, C., "Forensic materials engineering: case studies", Pages 1-429, CRC Press, Boca Raton, 2003.

22. Edelman, G.J., Hoveling, R.J.M., Roos, M., Leeuwen, T.G. van, Aalders, M.C.G., "Infrared imaging of the crime scene: possibilities and pitfalls", Journal of Forensic Sciences, Vol. 58, Issue 5, Pages 1156–1162, 2013.

23. Ammer, K., Ring, E.F.J., "Application of thermal imaging in forensic medicine", The Imaging Science Journal, Vol. 53, Issue 3, Pages 125-131, 2005.

24. Faltaous, S., Liebers, J., Abdelrahman, Y., Alt, F., Schneegass, S., "VPID: towards vein pattern identification using thermal imaging", i-com, Vol. 18, Issue 3, Pages 259–270, 2019.

25. Brooke, H., Baranowski, M.R., McCutcheon, J.N., Morgan, S.L., Myrick, M.L., "Multimode imaging in the thermal infrared for chemical contrast enhancement. part 3: visualizing blood on fabrics", Analytical Chemistry, Vol. 82, Issue 20, Pages 8427–8431, 2010.

26. Brooke, H., Baranowski, M.R., McCutcheon, J.N., Morgan, S.L., Myrick, M.L., "Multimode imaging in the thermal infrared for chemical contrast enhancement. part 1: methodolgy", analytical chemistry, Vol. 82, Issue 20, Pages 8412–8420, 2010.

27. Liu, J., Wang, C., Su, H., Du, B., Tao, D., "Multistage GAN for fabric defect detection", IEEE Transactions on Image Processing, Vol. 29, Pages 3388–3400, 2019.

28. Yildiz, K., Buldu, A., Demetgul, M., Yildiz, Z., "A novel thermal-based fabric defect detection technique", The Journal of The Textile Institute, Vol. 106, Issue 3, Pages 275–283, 2015.

29. Hamdi, A.A., Fouad, M.M., Sayed, M.S., Hadhoud, M.M., "Patterned fabric defect detection system using near infrared imaging", 2017 Eighth International Conference on Intelligent Computing and Information Systems (ICICIS), Pages 111–117, Cairo, 2017.

30. Scott, I.G., Scala, C.M., "A review of non-destructive testing of composite materials", NDT International, Vol. 15, Issue 2, Pages 75–86, 1982.

31. Raj, B., Jayakumar, T., Thavasimuthu, M., "Practical non-destructive testing", Pages 1-184, Woodhead Publishing, Cambridge, 2002.

32. Qu, Z., Jiang, P., Zhang, W., "Development and application of infrared thermography non-destructive testing techniques", Sensors, Vol. 20, Issue 14, Pages 1-26, 2020.

33. Zhao, Z., "Review of non-destructive testing methods for defect detection of ceramics", Ceramics International, Vol. 47, Issue 4, Pages 4389–4397, 2021.

34. Beveridge, A., "Forensic investigation of explosions", Pages 1-512, CRC Press, London, 1998.

35. Klastersky, J., Schimpff, J., Senn H.-J., "Collection of evidence", 35. Klastersky, J., Schimpff, J., Senn H.-J. et al editors, Practical homicide investigation: tactics, procedures, and forensic techniques, fourth edition, Pages 571-623, CRC Press, New York, 2006.

36. Casey, E., "Handbook of digital forensics and investigation", Pages 1-559, Elsevier Academic Press, Burlington, 2009.

37. Kobilinsky, L.F., "Forensic chemistry handbook", Pages 1-501, A Jonh Wiley & Sons, Inc., New Jersey, 2012.

38. Thorp, J., Smith, G.D., "Higher categories of soil classification: order, suborder, and great soil groups", Soil Sciences, Vol. 67, Issue 2, Pages 117–126, 1949.

39. Dizdar, M.Y., "Türkiye'nin toprak kaynakları", Pages 1-317, TMMOB Ziraat Odası Mühendisleri Odası Teknik Yayınlar Dizisi, Ankara, 2003.

40. Visioli, A., "Practical PID control", Pages 1-309, Springer, London, 2006.

41. Reprap, "RAMPS 1.4", https://reprap.org/wiki/RAMPS_1.4, March 18, 2020.

42. Altman, N.S., "An introduction to kernel and nearest-neighbor nonparametric regression", The American Statistician, Vol. 46, Issue 3, Pages 175–185, 1992.

43. Quinlan, J.R., "Induction of decision trees", Machine Learning, Vol. 1, Pages 81–106, 1986.

44. Breiman, L., "Random forests", Machine Learning, Vol. 45, Pages 5–32, 2001.

45. Liaw, A., Wiener, M., "Classification and regression by random forest", R News, Vol. 2, Issue 3, Pages 18–22, 2002.

46. Bertoni, A., Campadelli, P., Parodi, M. A, "Boosting algorithm for regression", ICANN 1997: International Conference on Artificial Neural Networks, Pages 343–348, Berlin, 1997.

47. Freund, Y., Schapire, R.E., "Experiments with a new boosting algorithm", Machine Learning: Proceedings of the Thirteenth International Conference (ICML'96), Pages 148–156, Bari, 1996.

48. Kohavi, R., "A study of cross-validation and bootstrap for accuracy estimation and model selection", Appears in the International Joint Conference on Artificial Intelligence (IJCAI), Pages 1137–1145, Montreal, 1995.

49. James, G., Witten, D., Hastie, T., Tibshirani, R., "An introduction to statistical learning with applications in r", Pages 15-419, Springer, New York, 2013.

50. Alpaydin, E., "Introduction to machine learning", Pages 1-407, The MIT Press, Cambridge, 2004.

51. Korkmaz, A., Büyükgöze, S., "Sahte web sitelerinin sınıflandırma algoritmaları ile tespit edilmesi" [Detection of Fake Websites by Classification Algorithms] [article in Turkish], Avrupa Bilim ve Teknoloji Dergisi, Vol. 16, Papes 826–833, 2019.

52. Luque, A., Carrasco, A., Martín, A., de las Heras, A., "The impact of class imbalance in classification performance metrics based on the binary confusion matrix", Pattern Recognition, Vol. 91, Issue C, Pages 216–231, 2019.

53. Kira, K., Rendell, L.A., "The feature selection problem: traditional methods and a new algorithm", AAAI-92, Pages 129–134, California, 1992.

54. Kira, K., Rendell, L.A., "A practical approach to feature selection", Machine Learning 1992, Pages 249–256, Aberdeen, 1992.

55. Kononenko, I., Šimec, E., Robnik-Šikonja, M., "Overcoming the myopia of inductive learning algorithms with relieff", Applied Intelligence, Vol. 7, Pages 39–55, 1997.

56. Hock, C.W., Sookne, A.W., Harris, M., "Thermal properties of moist fabrics", Textile Research, Vol. 14, Issue 5, Pages 144–149, 1944.